A Ground Truth Data Set for Nikon Camera's Spectral Sensitivity Estimation

Maryam Mohammadzadeh Darrodi, Graham Finlayson, Teresa Goodman, and Michal Mackiewicz*

School of Computer Science, University of East Anglia, Norwich, Norfolk, United Kingdom

**National Physical Laboratory, Hampton Road, Teddington, London, United Kingdom*

Abstract

Camera spectral sensitivity functions are obtained either by measurements in the laboratory or via estimation algorithms. A procedure for camera spectral sensitivity measurement is explained in this article, which aims to provide high accuracy ground-truth values with known uncertainty. The measurements were carried out on a Nikon D5100 camera at the National Physical Laboratory, London.

We use the obtained ground truth spectral sensitivity functions to evaluate the performance of some estimation algorithms reported in the literature. We conclude that the estimated sensitivities are not as accurate as the ground truth spectral sensitivities and further improvements are required. We validate previous work, which shows that a known camera basis provides a powerful constraint for estimation.

We have made the ground truth spectral sensitivities measured at NPL along with the detailed uncertainty levels available online for the community to use as a reference data set.

Introduction

The knowledge of camera spectral sensitivities is useful in many applications for example illuminant estimation [1], color correction [2, 3] and multispectral imaging [4, 5]. Camera manufacturers do not provide this data and so it is the user's task to either measure [6] or estimate their camera's sensor sensitivities.

In this paper, we describe a camera calibration procedure using a monochromator at the National Physical Laboratory (NPL), the UK national measurement institute. The novelty of this approach arises from the calibration set up which allows us to report the measured spectral sensitivities along with the measurement uncertainties. The stated uncertainty values are a combination of camera and calibration uncertainties and are reported per measured wavelength. These values help us understand how close the measured sensitivity values are to the actual camera sensor sensitivity functions. To our knowledge, prior calibration procedures discussed in the literature follow a much simpler set up, with less controlled conditions that may be easier and faster in practice [7-10] but do not address uncertainties. Our motivation is to provide the community with an accurate ground truth measured dataset, which aids the development of algorithms for spectral sensitivity estimation.

Secondly, we review spectral sensitivity estimation techniques. Despite the linearity of the image formation, one of the main difficulties of estimation techniques is the limited dimensionality of the reflectance spectra and the presence of noise in the measurements meaning that the problem is ill-posed [11, 12]. In this article we review a number of regression based estimation algorithms including Tikhonov regularization [13, 14], Tikhonov based on derivatives [15], simple linear regression where the spectral sensitivities are assumed to lie in the basis of a linear model of small dimension [7, 16] and quadratic programming [17]. We compare their performance with the NPL ground truth spectral response functions based on real measured data from the Macbeth colour checker. We use three different error metrics for evaluation and comparisons of these techniques.

In next section, we present the background necessary for understanding camera calibration models with brief explanations of spectral sensitivity recovery methods. Sensor sensitivity measurements at NPL followed by details of the evaluations of the associated calibration uncertainties are explained after that. Validation tests along with results on the estimation errors are discussed in the results section and finally we conclude.

Background

Mathematically, the simplest color formation model for the i^{th} sensor and j^{th} pixel response p_i^j can be written as:

$$p_i^j = \int_\omega E(\lambda)\, S_j(\lambda) Q_i(\lambda) d\lambda, \qquad i = 1,2,3 \tag{1}$$

where $E(\lambda)$ is the spectral power distribution of the scene illuminant, $S_j(\lambda)$ is the surface reflectance imaged at pixel j and $Q_i(\lambda)$ is the spectral response of the sensor i. By sampling spectral quantities at 10nm intervals over the visible spectrum, the integral in (1) can be replaced by a summation over the m intervals ($m = 31$ in the example case where sampled at 10nm) transforming Equation (1) to (2),

$$p_i^j = \sum_{l=1}^{m} E(\lambda_l) S_j(\lambda_l) Q_i(\lambda_l) \Delta\lambda, \quad i = 1,2,3 \tag{2}$$

where the scalar $\Delta\lambda$ denotes the nanometre sampling difference. By assuming $q_{il} = Q_i(\lambda_l)\Delta\lambda$ and $c_{jl} = E(\lambda_l)S_j(\lambda_l)$ for a single pixel and one sensor channel (2) can be transformed into (3) which can be written in vector notation as follows:

$$p = \underline{c}^t \underline{q}, \tag{3}$$

Assuming we have n known reflectance –i.e mxn matrix S - under a known illuminant we can write the n responses, $\underline{P}$ for each sensor as:

$$\underline{P} = C\underline{q}, \quad (4)$$

where C is called the nxm color signal matrix, in which $\underline{c_j}^t$ is the j^{th} row. When $n \geq m$ and C is full rank, C^tC is invertible and minimizing the sum of squares error between the sensor responses and their estimate, using the standard – closed-form – Moore Penrose invers *[18]* estimates a solution for $\underline{q}$,

$$min_{\underline{q}} \left\| C\underline{q} - \underline{P} \right\|^2 \Rightarrow \underline{q} = [C^tC]^{-1}C^t\underline{P}. \quad (5)$$

When $n < m$, one condition is where the matrix is not invertible and there is an infinite number of solutions. In this case we assume that the sensor $\underline{q}$ is in the space of the reflectance and so we have the following solution:

$$\underline{q} = C^t[CC^t]^{-1}\underline{P} \quad (6)$$

Of all sensors that solve (5) exactly, the solution in (6) is the solution with least norm. However, often using (6) or (5) on real data results in poor recovery (jaggy sensors) and simple regression fails. Further the problem is not solved given more data. Indeed because reflectance are ultimately smooth the cross product matrix C^tC will in general be 'almost' not invertible [19]. Practically, this means that very small perturbations in the measurements of $\underline{P}$ can result in large differences in the estimated sensors. Thus we turn our focus to spectral sensitivity recovery algorithms that are directed toward making the regression more stable. In summary these algorithms use one or a combination of the criteria illustrated in Table 1.

Table 1: Table of summary formulae for the sensor sensitivity estimation algorithms. B is the $m \times h$ matrix of basis functions, $\underline{a}$ is the h element vector of coefficients, γ is the regularization parameter determined for minimizing the norm of the solution and T is a second order derivative operator in matrix form.

I	Regularization	$\min_{\underline{q}}(\left\| C\underline{q} - \underline{P} \right\|^2 + \gamma \left\| T\underline{q} \right\|^2)$
II	$\underline{q}$ is a linear combination of basis functions i.e. $\underline{q} = B\underline{a}$	$\min_{\underline{a}} \left\| CB\underline{a} - \underline{P} \right\|^2$
III	Linear constraints Posivity: Uni-modality:	$\underline{q} \geq 0$ $q_l \leq q_{l+1},\ l = 1, \dots, z-1$ $q_l \geq q_{l+1},\ l = z, \dots, m$

Tikhonov regularisation [13] follows (I) when T is equal to the identity matrix. It adds a penalty term to the normal least-squares error in order to prevent jaggy (high norm) sensor recoveries. Here we use the L-curve criterion [14] to find a γ that minimizes both the recovery error and norm of the sensor using:

$$\underline{q} = [C^tC + \gamma T^tT]^{-1}C^t\underline{P}, \quad (7)$$

Dyas proposed to apply T as the discrete second order derivative operator matrix [15] turning (I) to semi-norm minimization which imposes a smooth solution to (7). Again the L-curve criterion is applied for finding the best γ [14]. Note that (7) is explicitly the solution to (I).

Minimisation (II) points to adapting a set of linear basis (in which spectral sensitivity must lie). By this in (2) we assume:

$$Q(\lambda) = \sum_{k=1}^{h} a_k B_k(\lambda) \quad (8)$$

where $B_k(\lambda)$ denotes the basis as a function of wavelength λ and a_k is its coefficients. Choices of $B_k(\lambda)$ discussed in this article are summarized in Table 2. Also we use linear models that are derived directly from the Principal component analysis (PCA) of 28 different camera's real measured spectral sensitivities by Jiang et al. [7] and Gu [20].

Table 2: Forms of $B_k(\lambda)$ applied by Radial, Sine and Fourier basis to (8). Where μ indicates the center of the radial basis weighted by an appropriate coefficient σ.

Radial	Sine	Fourier
$exp\left(-\frac{(\lambda - \mu_k)^2}{\sigma^2}\right)$	$sin\,(k\lambda\pi)$	$sin\,(k\lambda\pi) + cos\,(k\lambda\pi)$

Substituting (8) into matrix form we write

$$\underline{q} = B\underline{a} \quad (9)$$

where $\underline{a}$ is a result of minimizing (II) in Table 1. Sensor estimation using (II) subject to (III) when B is the matrix of Fourier series basis functions can be implemented by quadratic programming [17] where additional constraints are employed.

In this paper we benchmark the performance of existing published algorithms and compare them with ground truth data. We refer the reader to the original research articles for further details on the algorithms.

National Physical Laboratory Spectral Sensitivity Measurement System

In this section we provide a detailed description of the detector spectral sensitivity calibration facility of the National Physical Laboratory in London. The system consists of a tungsten halogen lamp, a double monochromator, which selects a narrow band of wavelengths from the lamp, and optics, which direct the emergent optical radiation from the monochromator to either a reference silicon photodiode or the camera being calibrated (see Figure 1). The optics are housed within a blackened enclosure, which prevents ambient light from reaching the detectors, and baffles are used to reduce the effects of any scattered light within the enclosure as illustrated in Figure 1.

The system is based on the principle of substitution, in which the silicon reference detector (monitored by Lab computer) is irradiated from the monochromator which was set to the required wavelength. Then a white tile is moved into the beam (by means of the translation slide), in order to provide a uniform radiance field which was then imaged by the camera (monitored by laptop). The reflectance of the white tile in the 0/45 geometry used (i.e. irradiation at 0°, viewing at 45°) was calibrated at NPL and was allowed for when determining the sensitivity of the camera [21]. The main shutter was then closed blocking the beam coming from the monochromator, and a dark image of the tile was captured with the camera. Finally, the monochromator was set to the next wavelength and the process repeated.

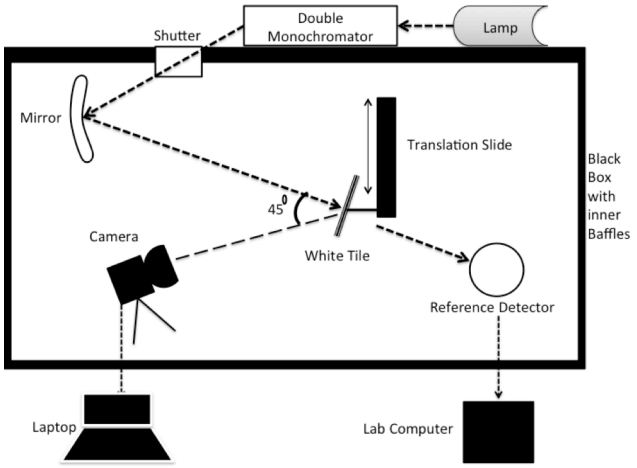

Figure 1: Illustration of the calibration set up of the NPL Automated spectral sensitivity measuring system and test camera.

The radiance is measured using the reference silicon photodiode whose sensitivity at each wavelength has been calibrated against SI units [22], allowing for the reflectance of the tile. This is denoted by L_l for the l^{th} wavelength and (assuming that the diffuser behaves as an ideal cosine reflector) is calculated using

$$L_l = p'_l \partial_l / q'_l \pi \ , \quad (10)$$

where p'_l is the dark corrected signal from the reference detector, q'_l is the calibrated irradiance sensitivity of the reference detector and ∂_l is the reflectance of the white tile. Thus the absolute spectral radiance sensitivity for a camera sensor (R, G or B) at wavelength l, denoted as q_l^A, can be calculated using

$$q_l^A = p_l / L'_l, \quad (11)$$

where p_l is the dark corrected camera signal of the sensor, which is derived by subtracting the dark camera signals from light signals and averaging over the central area of the captured images.

Note that Equation 11 relates to the absolute spectral radiance sensitivity of the camera sensor expressed in units of signal per Watt per metre squared per Steradian. Absolute spectral sensitivity measurements would require the substitution of the reference detector and the white tile to be made in the same plane at the focus of the mirror, in which position the irradiated area was relatively small and non-uniform. In practice, lower calibration uncertainties could be achieved by working in terms of relative spectral sensitivities, which meant that the white tile could be placed closer to the mirror (rather than being placed in the same location as reference detector) as shown in Figure 1, generating a larger and more uniform measurement area onto which the camera was focused. The camera signal value was therefore normalized by the maximum signal for each channel before performing the calculation given in Equation 11, yielding the relative spectral sensitivity function; note this is dimensionless, i.e. has unit = 1.

Nikon D5100 was calibrated using this system. Measurements were made over the wavelength range 380 nm to 770 nm, at 5 nm intervals. The camera readings were averaged over a 21×21 pixel patch in the centre of the image, in order to reduce the effects of noise on each pixel. After initial experiment on camera exposure determination, we decided to use 15s exposure time with full aperture over the visible range along with repeating the measurements in the region of 580 nm to 630 nm for the red channel with faster shutter speed (5s) in order to recover the lost information due to saturation for that channel. The ratio of the two shutter speeds (r=3) is used to stitch the two data sets (15s and 5s) together.

The NPL calibration included a full evaluation of the calibration uncertainty. These can be summarized as follows:

- **Uncertainty associated with the Reference detector.** This arises from the uncertainty associated with the calibration of the reference detector by comparison with the NPL spectral responsivity scale and additional uncertainties that arise due to possible drift in the detector between its time of calibration and time of use. The combined 2σ uncertainty for these two effects varies from about 0.6% at 380 nm to less than 0.2 % for wavelengths from 500 nm to 800 nm [23].
- **Uncertainty associated with the spectral reflectance of the white tile.** This arises from the calibration of the white tile on the NPL National Reference Reflectometer in the 0/45 geometry used and drift in the reflectance since the time of calibration, and is 0.75% for wavelengths between 400 nm and 800 nm, increasing to 1.35% for shorter wavelengths [21].
- **Uncertainty associated with the NPL spectral responsivity facility.** This includes uncertainties arising from stray light scattered within the measurement enclosure, wavelength uncertainty of the monochromator, noise and drift of the light source and reference detector, measurement repeatability, etc. These effects have been pre-measured at NPL and reports show an uncertainty of about 0.8% for the transfer of the calibration from one detector to another in the configuration used for these measurements.
- **Uncertainties associated with the camera.**
  - **Uncertainty due to scaling factor**. The uncertainty associated with stitching the two data sets (15s and 5s) with scaling factor r was determined around 3% which was only applicable for wavelengths between 580 nm to 630 nm for Nikon's red sensor. This uncertainty for other wavelengths and other sensors is zero.
  - **Uncertainty due to non-uniformity effects.** As mentioned earlier, we averaged the pixel response p^j over the calibration area. The uncertainty due to pixel to pixel variations of the pixel response p^j can be calculated from the following for each sensor:

$$\frac{\sigma/\sqrt{n}}{\overline{p}} \quad (12)$$

where n is the number of pixels in the calibration area (which is 21×21 pixels), $\overline{p}$ is average of the dark corrected signal (over the 21 pixel × 21 pixel area), and σ is the standard deviation of p^j over the calibration area of the dark corrected image. The outcome of dividing the standard error of the mean by the averaged signal is the relative non-uniformity uncertainty for that wavelength.

  - **Uncertainty due to dark noise.** This uncertainty was measured in the same way as the non-uniformity

except that the standard error was obtained from the dark reading images taken at each wavelength (σ_{dark} in Equation 12) resulting in the relative dark noise uncertainty for that wavelength.

- **Uncertainty associated with camera repeatability.** This was evaluated by capturing 10 images of the same scene (Macbeth color checker illuminated by the illuminant D65). For each data set, the maximum standard deviation of the dark-corrected camera signals of the achromatic colors across the 10 images was used in Equation 12 (with n =10) to result in the relative standard uncertainty associated with camera repeatability (see Table 3).
- **Uncertainty associated with sensor non-linearity.** This uncertainty was evaluated by plotting the camera signals against the achromatic sample reflectance of a Macbeth color checker illuminated by the D65 illuminant for three different levels of exposure: 1/40s, 1/25s and 1/15s see Figure 4. The maximum separation of the points from the ideal straight line in this graph is treated as the bounds of a rectangular uncertainty distribution function, so allowing the standard uncertainty associated with camera non-linearity to be evaluated using (12) with $n = 3$ when R, G and B are between [0,1] (see results in Table 3).

Table 3: Table of linearity and repeatability uncertainty percentages for Nikon camera. The values in this table are relative uncertainty percentages that are assigned to all measured wavelengths.

	Linearity	Repeatability
R	0.06	0.07
G	0.08	0.05
B	0.16	0.06

The root of sum of squares of the camera relative uncertainties listed above is calculated to estimate the total camera uncertainty. Finally the root of sum of squares of the relative uncertainties associated with the reference detector, white tile, responsivity facility and camera is calculated to give the uncertainty value for the entire calibration process. Figure 5 in the Appendix illustrates the detailed uncertainty values for every wavelength of Nikon's red sensor response. Figure 2 illustrates the measured spectral response function of the Nikon camera, with error bars marking the uncertainties that are higher than 0.5% for the high frequency region of 450 to 650nm. This graph is a simple illustration of the benefit of the calibration approach at NPL showing low levels of uncertainties for the camera which marks a robust source, reliable enough to be evaluated and applied as ground truth data for comparison purposes in the next section. Full uncertainty data are available online.

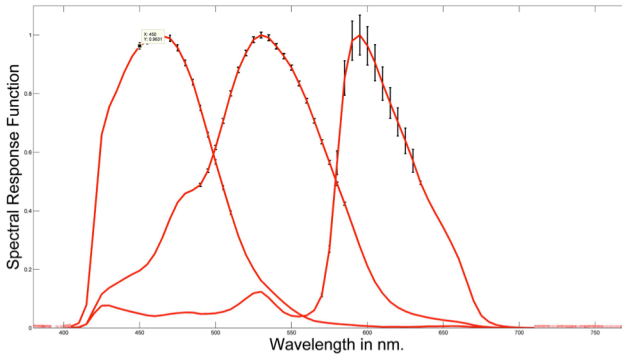

Figure 2: Measured Nikon camera sensitivities from NPL calibration. Uncertainity levels over 0.5% are illustrated with black error bars across the high frequency region of 450 to 650nm.

Experiments and Results

4.1 Validation of NPL measured spectral response functions (outside NPL)

First, outside the lab, we wish to compare measured RGBs to those predicted by the numerical integrations of the NPL measurements. So we take a picture of the 24 patch Macbeth colour checker [24] and compare the camera response with the 24 colour signals spectrally mapped to RGBs using (1).

Real data: Macbeth color checker [24] was placed in the center of the floor of a VeriVide cabinet, facing upwards towards the D65 illuminant. The position of the camera relative to the color checker was chosen to be approximately at 45 degrees. For each patch in the checker, the camera signal was obtained by averaging the dark corrected images for each of the red, green and blue channels over the central area of the patch resulting in $P_{24\times3}$ matrix.

Estimated data: A PR650 was set in the same position as the camera explained for real data collection (approximately at 45 degrees relative to the color checker placed in a VeriVide cabinet) to obtain measured $C_{24\times31}$. Note that, rather than moving the PR650 the Macbeth colour checker was moved into center of PR650's focus for each colour patch measurement in order to keep the light intensity constant across all 24 samples. Then $\hat{P}_{24\times3}$ is numerically calculated using (5).

Prior to comparison, all rows of $\hat{P}$ and P are divided by the corresponding RGB values of the white in that matrix. As a result both matrices would have values equal to one for R, G and B (i.e. for each channel response we would have p_j/p_{white}, j=1,..24). Relative estimation error for each R, G or B channel's response $\underline{p}$ and estimated response $\underline{\hat{p}}$ is calculated as:

$$E = 100\times(\left|\underline{p} - \underline{\hat{p}}\right|/\left|\underline{p}\right|) \quad (13)$$

Results in Table 4 illustrate the average relative prediction error percentages is 1.5%, correlating with less than 3 CIE Lab Delta E values.

Table 4: Mean prediction error of the validation experiment (outside NPL) for the measured spectral sensitivity functions in percentages.

	R	G	B	Average
Nikon	1.4	1.4	1.6	1.5

4.2 Evaluation and comparisons of sensor's spectral sensitivity estimation algorithms

The estimation algorithms tested have parameters to be tuned. The results reported are for the optimal parameters we found. Estimation error is computed in three ways. Spectral error is calculated as:

$$SE = 100\times(\left|\underline{\hat{q}} - \underline{q}\right|/\left|\underline{q}\right|) \quad (14)$$

where for each channel, $\underline{q}$ is $m\times 1$ and denotes a single sensor's measured spectral sensitivity (from NPL) and $\underline{\hat{q}}$ denotes the estimated spectral sensitivity re-scaled regarding to $\underline{q}$ using the following:

$$\underline{\hat{q}} = \underline{\hat{q}}(\max\left(\underline{q}\right)/\max\left(\underline{\hat{q}}\right)) \quad (15)$$

Spectral error is a pessimist measure, which in effect, measures only chromatic signals that are monochromatic lights. Vora and Trussell's [25] value captures the difference in spectral response for all possible colour signals. They show this estimate can be found by calculating

$$Vora = 100\times(1 - (trace(QQ^{+}\hat{Q}\hat{Q}^{+}))/3) \quad (16)$$

in which $\hat{Q}^{+}$indicates the Moore Penrose inverse [18] illustrated in (5) and dg is an operator that returns the diagonal elements of the matrix. Vora values close to 0 indicate estimated sensors close to measured ground truth.

The results of evaluating the estimation algorithms using (13) are illustrated in the first column of Table 5 followed by averaged values of SE from (14) and Vora from (16).

Table 5: Table of percentage errors. Numbers accompanying the estimation technique names represent the number of basis used.

Estimation Method	Averaged E	Averaged SE	Vora
Tikhonov	1.4	16	3.0
Tikhonov on derivatives	1.4	17	2.9
Radial-7	1.2	42	13.7
Sine basis-7	1.1	18	2.7
PCA Basis-2	2.1	10	0.8
QP-5	1.2	22	3.9

4.3 Discussion

Comparing the averaged E values of Table 4 with Table 5 we can see that most estimation algorithms provide plausible predictions for the camera response imposing true validations.

We compare each estimation technique by looking at the averaged SE and Vora's values in Table 5. PCA with 2 basis works best while sine basis, Tikhonov, Tikhonov on derivatives and quadratic programming perform moderately and radial basis performs worst. For simplicity in Figure 3 we choose to illustrate best and worst estimation techniques for the red sensor. PCA with 2 basis provides close estimates to the NPL ground truth data since the initial basis derived from 28 calibrated Nikon and Canon Cameras [7, 20] are similar in shape to the ground truth sensors. Radial basis results in jaggy spectral response. Thus, further development of these estimation techniques is required. Also the question of whether these methods would perform similarly well when exposed to other types of camera (such as Sigma) or synthetic data sets is what we will be addressing in the next publications to come.

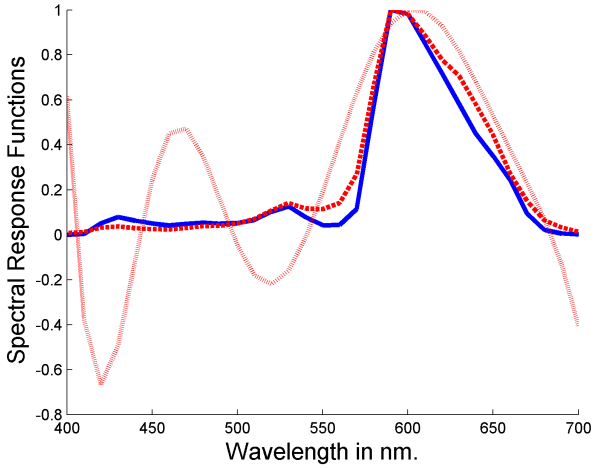

Figure 3: Illustration of the red channel spectral response function recovered from NPL (solid line), estimated uing PCA on 2 basis (dashed) and radial basis (faint line) using real data from Macbeth color checker.

Conclusion

In this paper we have described the methodology for measuring the spectral response functions for Nikon D5100 camera at the National Physical Laboratory. We explained how the spectral response functions can be measured using the calibration system and a reference detector with a calibration that is traceable to SI units. We determined approximately 2% uncertainty for the recovered spectra per wavelength, and validated with only 1.5% relative response prediction error. This data is made available for the community as reference ground truth data set.

Various sensor sensitivity estimation techniques are implemented, validated and compared with the ground truth spectra of the Nikon camera. The results based on Nikon's data show that PCA with 2 basis on previously measured camera sensors estimate sensors very close to the ground truth and further improvements are required for the rest of the estimation techniques. Thus we hope that by making the ground truth data available we aid this aim. Further measurements and evaluations of more estimation techniques on other cameras will be discussed in future publications.

Acknowledgments

With thanks to Subrena Harris at NPL. Data are available for download at: http://spectralestimation.wordpress.com/data/

Appendix

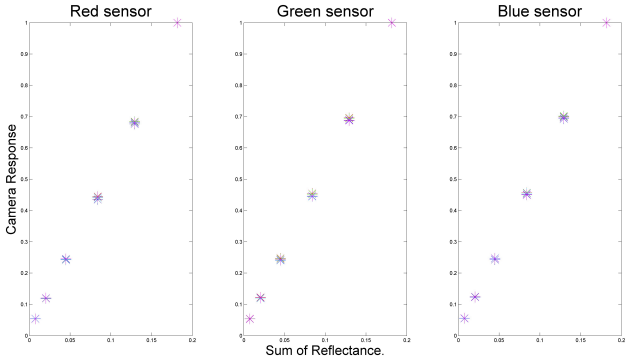

Figure 4: Figures of linearity test for Nikon camera. Points represent the camera signal in response to the input mean reflectance for 1/40s, 1/25s and 1/15s exposure timings.

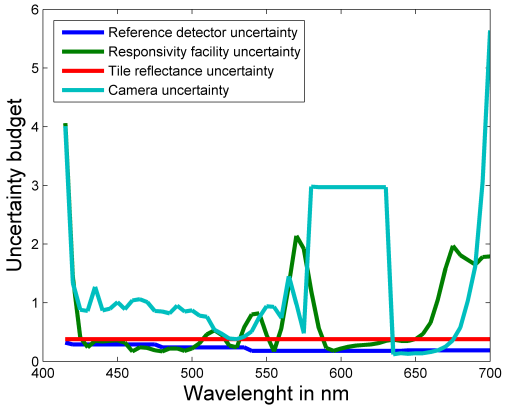

Figure 5: Uncertainty budget percentages for Nikon's red channel spectral response function.

References

1. G.D. Finlayson, P.M. Hubel, and S. Hodley, Color by correction. Proceedings of the Fith Color Imaging Conference: Color Standards and Color Measurements. pg. 6, (1997).
2. G.D. Finlayson and M.S. Drew, White-point preserving colour correction. Proceedings of the Fith Color Imaging Conference: Color Standards and Color Measurements. pg. 258, (1997).
3. G.D. Finlayson and M.S. Drew, "Constrained least-squares regression in color space," Journal of Electronic Imaging. 484, (1997).
4. N. Shimano, K. Terai, and M. Hironaga, "Recovery of spectral reflectances of objects being imaged by multispectral cameras," Journal of Optical Society of America A. 24(10), pg. 3211, (2007).
5. F.H. Imai and R. Berns, Spectral Estimation Using Trichromatic Digital Cameras. Proceedings of International Symposium on Multispectral Imaging and Color Reproduction for Digital Archives, (Society of Multispectral Imaging). pg. 42, (1999).
6. ISO, Graphic technology and photography — Colour characterisation of digital still cameras (DSCs) in Part 1: Stimuli, metrology and test procedures. (2012).
7. J. Jiang, et al., What is the Space of Spectral Sensitivity Functions for Digital Color Cameras. IEEE Workshop on the Applications of Computer Vision. pg. 168, (2013).
8. P.L. Vora, et al., Digital color cameras - 2 Spectral response, in HP Technical Report. (1997).
9. J. Nakamura, Image Sensors and Signal Processing for Digital Still Cameras ed. (Micron: CRC Press, 2005), pg.
10. D.L. Bongiorno, et al., Spectral characterization of COTS RGB cameras using a linear variable edge filter, in IS&T/SPIE, Electronic ImagingInternational Society for Optics and Photonics: California, USA. pg. 86600N. (2013).
11. P.M. Hubel, D. Sherman, and J.E. Farell, A Compariosn of Methods of Sensor Spectral Sensitivity Estimation. Color Imaging Conference: Color Science, Systems and Applications. pg. 45, (1994).
12. Y.H. Hardeberg, H. Brettel, and F.J. Schmitt, "Spectral characterization of electronic cameras," Electronic Imaging: Processing, Printing, and Publishing in Color. 100, (1998).
13. A.N. Tikhonov and V.Y. Arsenin, Solution of Ill-posed Problems, ed. (Washington: Winston & Sons, 1977), pg.
14. P.C. Hansen and D.P. O'Leary, "The use of the L-curve in the regularization of discrete ill-posed problems," SIAM J. Sci Comput 14 1487, (1993).
15. B. Dyas, Robust color sensor response characterization. Eighth Color Imaging Conference. pg. 144, (2000).
16. H. Zhao, et al., Estimating basis functions for spectral sensitivity of digital cameras. Meeting on Image Recognition and Understanding. pg. 7, (2009).
17. G.D. Finlayson, S. Hordley, and P.M. Hubel, Recovering device sensitivities with quadratic programming. The Sixth Color Imaging Conference: Color Science, Systems, and Applications. pg. 90, (1998).
18. E. Moore, "On the reciprocal of the general algebraic matrix.," Bull Am Math Soc. 26 394, (1920).
19. G.H. Golub and C.F. Van Loan, Matrix computations, ed. (USA: Jhon Hopkins University Press, 1996), pg. 270-274.
20. J. Gu. Available from: http://www.cis.rit.edu/jwgu.
21. C.J. Chunnilall, et al., "NPL scales for radiance factor and total diffuse reflectance," 40 192, (2003).
22. J.E. Martin, N.P. Fox, and P.J. Key, "A Cryogenic Radiometer for Absolute Radiometric Measurements," Metrologia. 21 147, (1985).
23. N.P. Fox, "Trap detectors and their properties," Metrologia. 28 197, (1991).
24. C.S. McCamy, H. Marcus, and J.G. Davidson, "A color-rendition chart," Journal of Applied Photographic Engineering. 2(3), pg. 95, (1976).
25. P.L. Vora and H.J. Trussell, "Measure of goodness of a set of color-scaning filters," j. Opt. Soc. Am A. 10(7), pg. 1499, (1993).

Author Biography

Maryam Mohammadzadeh Darrodi joined UEA in 2012 where she was awarded Senior Research Associate role at the age of 26. Maryam has been trained in Statistics and has been awarded PhD from University of Leeds, school of Design in color science. She currently works at the color group closely with Professor Graham Finlayson and also Dr.Michael Mackiewicz who is also a Postdoc researcher at school of computer science. She has closely worked with Teresa Goodman at NPL labs for camera calibration.